Simultaneous Measurement of Surface and Bulk Vector Magnetization Dynamics in Thin Ni–Fe Films

Matthew R. Pufall and Thomas J. Silva, *Member, IEEE*

Abstract—The dynamics of the surface and "bulk" magnetization vectors of a Ni–Fe thin film were measured using the time-resolved second harmonic and linear magnetooptical Kerr effects. Films of 50, 250, and 400 nm thickness were measured. The magnetization dynamics of the surface and "bulk" in response to a pulsed torque field were effectively the same for all thicknesses, indicating that any induced eddy currents do not appreciably screen the interior of the film from the incident magnetic field at these thicknesses. The magnetization angle also showed both a large, fast (<1 ns) initial response to an applied field pulse, and then a slower (≫10–100 ns) "viscous" creep toward its dc value. Possible mechanisms for these observations are discussed.

Index Terms—Bulk magnetization, eddy currents, magnetization dynamics, magnetooptical Kerr effect, nickel–iron films, surface magnetization.

I. INTRODUCTION

AS DATA rates increase in modern magnetic storage devices, the writing and reading processes are beginning to require the movement of magnetization vectors at speeds at which precessional dynamics become important [1]. With this progress toward precessional processes in commercial applications, new strategies to optimize magnetic switching can be introduced. For example, fast reversal of a magnetic entity can be achieved by using "coherent control" of precessional motion—that is, using multiple pulses with particular direction and phase to apply torques to start and stop magnetization motion—rather than by domain formation or domain wall motion [2]. Large-angle motion of the magnetization $\vec{M}$ at these speeds is damped [denoted phenomenologically by α, the Landau–Lifshitz–Gilbert damping parameter (LLG)], and can also involve spin wave generation. In addition, eddy currents are increasingly induced at higher frequencies in a conducting medium. Eddy currents are believed to cause precessional damping and flux attenuation in the bulk of the film [3]–[5]. Finally, due to their differing symmetries, the surface and bulk of the material have different local magnetic anisotropies, differences that may affect the temporal response of the total system.

Current theoretical predictions of the relative sizes of these effects are, however, quite model and parameter dependent. Direct measurements of the temporal dynamics of the magnetization vector of both the surface and the bulk during large-angle magnetization motion will help to develop a more adequate understanding of these effects. The magnetooptical Kerr effect has proven to be an effective tool for the time-domain measurement of magnetization dynamics [6]. In addition, it can be used to measure surface and bulk dynamics [7]. The linear magnetooptical Kerr effect (MOKE) probes the magnetization over more than an optical skin depth ($\delta_{\text{skin}} \sim 20$ nm for Ni–Fe), and as such at least partially probes the bulk magnetization vector [8]. The second-harmonic variant (SH-MOKE), on the other hand, measures only the magnetization of the first few atomic layers away from the surface (the surface is where inversion symmetry is broken, and so two-photon processes are permitted) [9]. To fully understand large-angle magnetization dynamics, one must measure the magnetization vector—both its direction and magnitude—rather than simply one component, to discriminate between changes due to inhomogeneous modes (spin waves), and coherent rotations of $\vec{M}$ [9]. MOKE and SH-MOKE in principle have sensitivity to both in-plane components of $\vec{M}$, and so are well-suited to study the vector magnetodynamics of these thin-film systems.

Previous measurements have compared surface and bulk responses. Silva *et al.* compared SH-MOKE temporal response to the inductive signal generated by the magnetization in response to pulsed-field excitation [10]. These measurements showed a difference between the two signals in a 75 nm Ni–Fe film. Though an interesting comparison, the two techniques measure markedly different magnetizations: SH-MOKE is a local probe of the surface magnetization, while the inductive signal is an average response due the entire sample's magnetization dynamics. As a consequence, the measurement was less a probe of surface and bulk than a probe of local and average magnetizations.

II. METHOD

A. Magnetooptical Geometry

A schematic of the system is shown in Fig. 1. In magnetooptical measurements, the plane formed by the incident and reflected beams (the plane of incidence) defines the sample coordinate system. For the optical beams, electric field vectors polarized in this plane are called "p"-polarized, and those polarized perpendicular to it "s"-polarized. The sample's magnetization vector is typically defined relative to this plane and the plane of the sample surface. The component of $\vec{M}$ lying in the plane of the sample, and in the plane of incidence is called the longitudinal component, while the component in the sample plane but perpendicular to the plane of incidence is called the transverse component. The component parallel to the surface normal is the polar component. In the measurements presented here, the polar
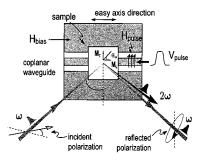
Fig. 1. System schematic, showing magnetooptical coordinate system, sample orientation, and coplanar waveguide structure to deliver high-speed magnetic field pulses. The center conductor width is ~450 μm.

component of $\vec{M}$ is small (a few percent of the in-plane $\vec{M}$) and is not measured.[1]

B. Surface Magnetization Measurements Using SH-MOKE

The basic physics of SH-MOKE has been discussed in detail elsewhere [12], [13]. Second-harmonic generation, the combination of two "fundamental" photons into a photon of twice the energy, occurs in media in which the normal modes of oscillation are not harmonic, that is, when linear superposition is no longer valid. Stimulation by a harmonic wave then excites oscillations that can mix harmonic modes. For crystal structures with inversion symmetry, the normal modes are harmonic to second order in the incident electric field $\vec{E}$ for electric dipole excitations, so second harmonics can be generated only at surfaces where this symmetry is broken. This is the origin of the surface sensitivity of SH-MOKE. Even in polycrystalline materials such as the Ni–Fe alloy thin films studied here, the vast majority of the second-harmonic light is produced at the surfaces of the film [14], [15]. Since high intensities are required to generate a detectable amount of second harmonic light (the intensity of the SH light produced scales as the square of the incident intensity, I_{incident}^2) an ultrafast pulsed laser is used, since these have extremely high peak powers, but deliver relatively low total energy to the sample, minimizing the thermal load. The brief duration of the laser pulses also permit time-resolved measurements.

The intensity and polarization of the second harmonic are also a strong function of the magnetization vector of the interface [12], [16]. When p-polarized light is incident on a magnetized interface, the intensity of the second harmonic light is proportional to the transverse component of the magnetization, and the polarization angle and ellipticity of the SH light is proportional to the longitudinal component of $\vec{M}$. In our geometry, the easy axis of the sample is roughly aligned with the longitudinal direction, and the hard axis roughly parallel to the transverse direction. The two magnetooptical effects are used to simultaneously measure the in-plane magnetization vector at the surface.

[1]SH-MOKE is, in fact, insensitive to the polar component of $\vec{M}$, whereas linear MOKE is, in principle, sensitive to it, in a way similar to the longitudinal component. The MOKE signal from a Landau–Lifshitz–Gilbert model of precessional response of $\vec{M}$ to an in-plane field pulse, was calculated to see if it would prove a problem, by using magnetooptical Fresnel reflection coefficients [11]. The expected polar signal is at most a few percent of the in-plane signals.

C. Bulk Magnetization Measurements Using Linear MOKE

The linear magnetooptical Kerr effect describes the change in the intensity and polarization state of an optical beam reflected from a magnetic sample. It is based on the same physical effects as the Faraday effect (circular birefringence and dichroism), but in the reflected beam. Due to the presence of the magnetization, the usual Fresnel reflection coefficients become a reflection matrix with off-diagonal elements [11]. Because of the finite skin depth of light, the reflected beam carries information not only about the magnetization of the sample's surface, but also about the magnetization of the material located roughly one optical skin depth beneath the surface.

There are three basic Kerr effects, named for the component of the magnetization to which they are sensitive: the transverse, longitudinal, and polar Kerr effects. These effects are functions of the input polarization and angle of incidence, and in principle allow measurement of the full magnetization vector [8]. The transverse MOKE is analogous to the transverse SH-MOKE signal described previously: a change in the transverse magnetization produces a change in intensity of an initially p-polarized light beam. Similarly, a change in the longitudinal component of the magnetization produces a change in the reflected polarization ellipticity and rotation angles.

To measure the magnetization vector, one could simply measure the intensity and polarization state of the reflected beam, as is done in SH-MOKE. However, unlike SH-MOKE, both the polarization changes and the fractional changes in the total intensity are quite small, typically ~10^{-3} to 10^{-4} for a full switch of the magnetization direction. Consequently, the transverse measurement is sensitive to small fluctuations in intensity. In the present system, these fluctuations turned out to be comparable to the signal size itself.

One can circumvent this by rotating the input polarization slightly from the purely p-direction. The transverse Kerr effect then induces a change in the polarization of the reflected beam, rather than simply an intensity change. This change in polarization is an odd function of the input polarization angle. In contrast, the change in polarization due to the longitudinal Kerr effect is an *even* function of the input polarization angle. So, by making two measurements, one on either side of p-polarization, and taking the sum and difference of the two signals, one can isolate the transverse and longitudinal Kerr effects from each other, thereby permitting a measurement of the in-plane magnetization vector.

D. Stroboscopic Technique

Most high-speed magnetooptical measurements employ a stroboscopic technique to achieve fast time resolution. A "one-shot" method is not feasible, since the light intensities required to get minimal signal to noise would damage or destroy the sample. In a stroboscopic measurement, the system is put in a well-defined initial state, set in motion with an applied stimulus, and its state sampled an interval of time later. The system is then reset to its initial state, again set in motion, and sampled at a slightly different interval of time later. Consequently, probabilistically evolving characteristics
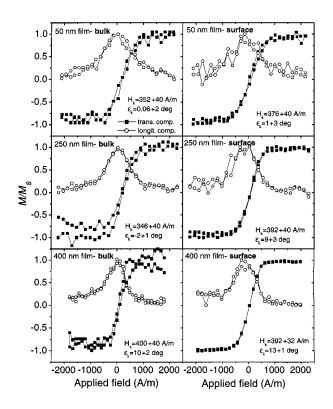
Fig. 2. Measured surface and bulk vector, dc hysteresis loops, for 50-, 250-, and 400-nm-thick films. Fitted values for the anisotropy field H_k and angle are given on the plots.

will be measured only in an average way. In magnetodynamical measurements this means, for example, that occasional domain formation could manifest itself as a decrease in the magnitude of the measured magnetization. Magnetization motion proceeding probabilistically via multiple trajectories could also result in such a measured decrease. We apply a bias field along the easy axis both to stabilize the magnetization (to inhibit domain formation), and to define a single ambient state to which the magnetization will return. The dc hysteresis loops taken (Fig. 2) show that the bias field is effective: Barkhausen jumps, which would be evidence for domain wall motion, are not visible, and the zero-field state is single-valued. Indeed, we find that the magnetization rotates coherently while the field is swept along the hard axis direction.

The MOKE/SH-MOKE instrument is based on a Ti : sapphire laser that delivers an 82-MHz optical pulse train with an average power of 1 W. This pulse rate is downsampled to 1 MHz using an electrooptic modulator and countdown electronics, enabling the use of commercially available pulse generators and coincident detection electronics with 1-MHz repetition rates. The excitation and detection electronics are synchronized to the laser pulse rate by diverting a small fraction of the optical beam to a trigger photodiode, producing a pulse that is electronically delayed by ~ 1 μs via coaxial delay line, so that the trigger pulse is roughly coincident with the arrival of the next laser pulse. A computer-controlled electronic delay controls the exact arrival time of this trigger pulse to the field pulse excitation electronics, and so controls the relative arrival of the magnetic excitation and optical pulses at the sample. In this way, the system provides temporal resolution, with a jitter-limited sensitivity of ~ 50 ps.

As shown in Fig. 1, the sample is mounted on a coplanar waveguide. A voltage pulse propagating down the center conductor produces a current in the conductor and a magnetic field around it. The field is largely parallel to the plane of the sample over the center of the waveguide. At the edges of the waveguide, the perpendicular field becomes comparable in size to the in-plane field, but the small perpendicular susceptibility of Ni–Fe thin films (1/50th of the in-plane susceptibility) makes this field a small perturbation on the dynamics. The waveguide is shorted to ground at its end. When the voltage pulse hits the short, it is both reflected back along the waveguide, and inverted in sign. This effectively doubles the field at the sample. The system in this configuration was capable of delivering ~ 1.5-kA/m (18 Oe) field pulses, with rise times of 150 ps.

In the measurement, the optical pulse is focused onto the sample using a microscope objective, at an angle of $\sim 45°$ to the surface normal. The reflected light (containing both the fundamental and SH wavelengths) is collected by another objective, and passes through a photo-elastic modulator and linear polarizer that together with a lock-in amplifier act as an ac ellipticity detector. A dichroic mirror is used to divert the fundamental light to the linear MOKE detector (described below), and pass the second harmonic light to a photon counting photo-multiplier tube (PMT). The PMT is connected to a coincident detection system that is synchronized to the 1-MHz laser repetition rate. The photon counting system is necessary because the second harmonic yield is quite small. The detection method is described in greater detail elsewhere [9].

The photoelastic modulator modulates both the second-harmonic and the fundamental light. Separate lock-in amplifiers are used to detect the ellipticities of each. The linear photodetector is a biased photodiode connected to a Schottky diode. This was used because the "closed" setting of the electrooptic pulse picker leaked a small amount of light (1/200th of each optical pulse). Since the small leakage was multiplied by 81, this proved to be a significant source of error on the linear signal (since the SH signal scales as I^2, the small leakage was insignificant). By setting the Schottky diode bias level so that only the 1-MHz pulses exceed the Schottky turn-on voltage, signals due to the leaking "blocked" pulses are not detected.

E. Calibration

To determine both the MOKE and SH-MOKE signals, three measurements were made with identical magnetic conditions, but with different input polarizations. The measurement at pure p-polarization gives the SH-MOKE response at the second harmonic wavelength (~ 400 nm), and information about the longitudinal component of $\vec{M}$ due to the linear MOKE at the fundamental wavelength (~ 800) nm. The two measurements on each side of p-polarization return the transverse and longitudinal linear MOKE signals. (Since the entire stroboscopic measurement technique presumes repeatability, this is essentially simultaneous measurement.)

The calibration procedure is similar for both MOKE and SH-MOKE [9]. At each angle, a hard-axis hysteresis loop is measured, with field applied by a pair of Helmholtz coils,

and a time-resolved trace also taken. A stabilizing bias field of 120 A/m (1.5 Oe) was applied along the easy axis for all the loops and time traces. For the linear MOKE signal, the transverse and longitudinal hysteresis loop signals are formed from the difference and sum of the loops swept at the biased input polarizations, due to the opposite symmetries of the transverse and longitudinal MOKE with input polarization, as described in Section II-C. The SH-MOKE loops are fit directly. These hysteresis loops are fit to a function that uses a Stoner–Wohlfarth coherent rotation model for the angle of $\vec{M}$. This results in a lookup table, relating the transverse or longitudinal signal to the magnetization component in that direction. When combined, the two signals give both the magnitude and direction of the magnetization in the film plane.

III. RESULTS AND DISCUSSION

A. DC Hysteresis Loops

Films of three different thicknesses (50, 250, and 400 nm) were studied in detail. These were made by sputter deposition in a dc magnetic field, to give them a uniaxial in-plane anisotropy. The films were first measured in an induction-field (B–H) looper. They showed the expected uniaxial behavior, with an anisotropy field $H_k \sim 360$ A/m, and a coercivity of $\sim$80–160 A/m. The vector dc hysteresis loops were then measured in the MOKE/SH-MOKE system. These are shown in Fig. 2. Both the surface and bulk hard axis (transverse) loops look similar to those measured with the B–H looper. Within the signal-to-noise level of the measurement, the loops show no discontinuous Barkhausen jumps that would indicate the existence of domains. Since the incident beam is focused to a $\sim$5–10 μm spot, nucleation, and movement of domains larger than this would appear as discontinuous large-angle switching events; domains smaller than this size would cause a smaller change, or a drop in overall signal amplitude. The fitted anisotropy field strength (H_k) and axis direction (ϵ_k) are shown for each set of loops, and are consistent with those obtained from the B–H loops.

The surface (SH-MOKE) and bulk (MOKE) loops are quantitatively similar. Both the anisotropy strength and the anisotropy axis direction are equal, within the uncertainty of the fit, for all film thicknesses. The 400 nm sample happened to be mounted slightly askew. This is reflected in the fitted anisotropy angles for both the surface and the bulk measurements. The results indicate that the surface of the film does not have an effective anisotropy that is grossly different from the effective bulk anisotropy.

B. Surface and Bulk Temporal Responses to Fast Field Pulses

Fig. 3 presents the motion of the magnetization vector in response to a $\sim$1450 A/m (18 Oe) magnetic field pulse directed along the hard axis (as shown in Fig. 1). For each film thickness, the angle of both the surface and bulk $\vec{M}$, relative to the plane of incidence (the longitudinal direction) are shown as a function of time. Because both components of the in-plane magnetization vector were measured, both the angle and the relative magnitude of the magnetization vector as a function of
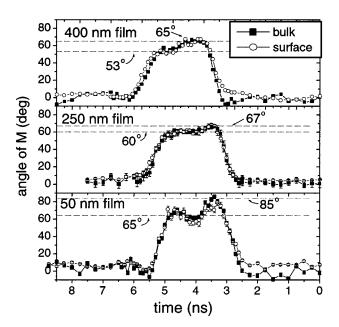

Fig. 3. Surface and bulk temporal response to hard axis magnetic field pulse, for 50-, 250-, and 400-nm-thick Ni–Fe films. Dashed lines indicate "peak" (maximum) and "saturation" (equilibrium) angles reached by $\vec{M}$ in response to the field pulse.

time were determined when calibrating the time response. $|\mathbf{M}|$ was found to be effectively constant with time, indicating that neither domains were formed, nor were appreciable numbers of short-wavelength spin waves generated during the rotation process.

These time traces have several features of note. First, up to the thickest film measured (400 nm thickness), the surface and bulk responses are quite similar. Both the rise time of the surface and bulk curves and the temporal undulations follow each other closely for all film thicknesses. Indeed, for all film thicknesses the initial rise times of the pulses are not appreciably different, within the temporal jitter-noise level ($\sim$50 ps rms) of the experiment.

Although the initial rates of response of the magnetization vectors in each of the films are similar, the "peak" (the maximum angle attained) and "saturation" (the angle reached just before termination of the pulse) angles of the magnetization vectors are not. These angles are indicated on the plots. Both the peak and saturation angles increase for decreasing film thickness. This was an unexpected result, since the films were all subject to magnetic field pulses of identical strength and have similar anisotropy fields and dc hysteresis loops. Consequently, one would expect near-identical rotations. Explanations for the differences in the magnetization rotation angles will be discussed in the next section.
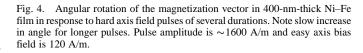
C. The Effect of Demagnetization Fields, and "Viscous" Temporal Response

Two effects contributed to the dependence of magnetization rotation angle on film thickness. The first effect is the generation of time-dependent demagnetizing fields within the sample. Due to the nonuniformity of the field from the waveguide, only the magnetization over the center conductor rotates appreciably. This inhomogeneity in the magnetization motion produces

demagnetizing fields. These fields impede the rotation of $\vec{M}$ and are larger for thicker films. Unlike the dc hysteresis loops, the field pulse for the time-resolved measurement is applied to a ~450–550 μm wide region over the waveguide. The coplanar waveguide fields can be calculated, to first order, using the Karlqvist equations for the fields of a semi-infinite pole head [17]. These equations apply also to a dc current in a finite-width current sheet. The calculated field profiles are sharp, slightly wider than the center conductor width at a height of 100 μm above the waveguide.

To measure the demagnetizing effects, a dc current was run through the waveguide center conductor and the magnetization response measured as a function of current strength. The slope of the hard-axis magnetization response with current gives an effective "current susceptibility" of the film. This susceptibility was measured as a function of position across the waveguide. The expected saturation response was determined by fitting the susceptibility as a function of position to an analytical model (the solution to Laplace's equation with appropriate boundary conditions, assuming linear magnetic media and subject to a potential distribution at the waveguide identical to that used to derive the Karlqvist equation). From this, one can determine the effective magnetic field as a function of position [17]. One finds that the effective susceptibility is indeed less than that obtained in a uniform applied field due to the induced demagnetizing fields.
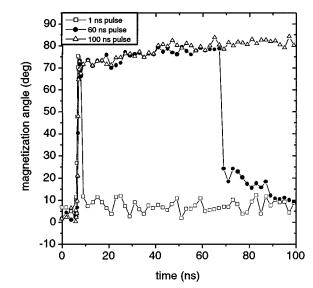
This demagnetization field will affect the final angle reached by the magnetization only if the applied field pulse is insufficient to saturate the film. However, we determined that the pulses applied to the thick films should still be more than sufficient to saturate the films, even with the induced demagnetization fields. An applied dc current of 1 A in the waveguide was sufficient to fully rotate $\vec{M}$ for the thickest film. The 40 V voltage pulse will induce a 1.8 A current, (determined from the characteristic impedance Z_0 of the waveguide, tested with 20-GHz instrumentation). Consequently, the magnetization should still rotate to near saturation during the 2 ns pulse, assuming that $\vec{M}$ rotates into an equilibrium state after precessional oscillations decay.

Though the magnetization angles in Fig. 3 appear to have reached equilibrium by the end of the pulse, measurements using longer duration pulses were made to see if the magnetization would continue to relax to a larger angle.[2] The temporal response of the angle of $\vec{M}$ to pulses of several widths are shown in Fig. 4. Note that for short times (<10 ns), highly damped precessional ringing occurs, as in the previous measurements, while for times longer than this, the magnetization angle slowly increases in a "viscous" manner out to 100 ns. Note, also, that the viscous component also manifests itself as a delayed restoration of $\vec{M}$ upon termination of the pulse: For the 60 ns

Fig. 4. Angular rotation of the magnetization vector in 400-nm-thick Ni–Fe film in response to hard axis field pulses of several durations. Note slow increase in angle for longer pulses. Pulse amplitude is ~1600 A/m and easy axis bias field is 120 A/m.

pulse, the magnetization angle takes many nanoseconds to relax to its initial value, while for the 1 ns pulse, the magnetization vector returns to its initial state almost immediately. From these results, we can say that the incomplete rotation observed for the 2 ns pulses (as compared to the measured dc rotation values) in the surface/bulk measurements is due to a slow viscous relaxation of the magnetization vector not accounted for by the simple, damped LLG precessional dynamics of a single magnetic domain that have been previously observed by time-resolved methods, and that given long enough pulse durations, the system would indeed approach the measured dc values [13].

Though this response can be broadly described as "viscous," the underlying mechanism (i.e., what is inducing the viscosity), is not known. Phenomenologically, corrugation of the energy surface traversed by $\vec{M}$ with many small local minima would approximate this response. In such a system, the magnetization would need the aid of thermal excitations to move the magnetization out of each local minimum toward its eventual saturation value. The behavior is not likely due to eddy currents, for the time constants (~50–100 ns) of the relaxation are far too long. A thermally assisted relaxation mechanism should have a strong dependence on applied field. Measurements were made of the relaxation rate as a function of pulse amplitude. The slow relaxation portion of the curves were fit to a function of the form $\theta_{dc} - \Delta \exp(-t/\beta)$. The final equilibrium angle θ_{dc} was calculated using the effective field (including demagnetization fields) and the Stoner–Wohlfarth model. The decay constant β showed no clear trend with pulse height, though was smallest for the largest pulse size. The amplitude Δ of the slow response, on the other hand, increased monotonically with decreasing pulse amplitude. The long times of the relaxation made an accurate determination of the viscous time scale difficult. Nevertheless, we can conclusively assert that the times exceed that expected for conventional LLG.

---

[2]These measurements were made in a linear MOKE system based on a pulsed laser diode, because the applied field pulse in the SH-MOKE system had a maximum duration of only 2 ns. The measurement method used was similar to that of the linear arm of the MOKE/SH-MOKE system. Since the wavelength of the laser diode (820 nm) was near that of the Ti : sapphire fundamental wavelength (800 nm), the optical skin depths of the two beams are comparable.

D. Comparison of Temporal Responses With a Simple Eddy Current Model

In a conductor, a changing magnetic flux will induce eddy currents. These currents act to oppose the change in flux. For a magnetic thin film, the changing flux is dominated by the motion of the magnetization itself, since $M_s \gg H_{\text{ext}}$. Furthermore, only the motion of $\vec{M}$ in the film plane induces appreciable currents, since any motion of $\vec{M}$ out of the plane will produce a demagnetization field equal and opposite to M_{perp}, making the total flux change $B_{\text{perp}} = \mu_0(M_{\text{perp}} + H_{\text{demag}}) \approx 0$. The magnitude of the eddy currents will increase with film thickness due to the increasing cross-sectional area and decreasing electrical resistance.

In a simple model for eddy current induction, one in which the magnetization is a linear function the local applied field H i.e., $\mathbf{B} = \mu \mathbf{H}$, the fields induced by eddy currents should screen the external field from the center of the magnetic material, the screening field increasing with depth into the sample. The rate of screening depends on the permeability and the resistivity of the material, and the thickness of the sample. These induced currents eventually decay due to the sample's electrical resistance, but serve to increase the rise time of the field in the center of the film. Consequently, if ferromagnetic exchange is ignored, the surface of the film should show a larger initial magnetization rotation than the bulk of the film, with the bulk lagging the surface slightly. Assuming that the local $\vec{M}$ is a linear function of the effective field $\mathbf{H}$, and using Ohm's law, one can derive a diffusion equation for the magnetic field in the magnetic material [4]. In a thin-film geometry subject an instantaneous step field pulse, the field at the surface is constrained to be H_0. Initially, the magnetic field within the film is zero, and increases progressively with time to H_0.

It is clear from the time traces shown in Fig. 3 that the bulk magnetization, insofar as it is probed by linear MOKE, does not initially lag the surface magnetization motion, and also reaches the same ultimate rotation angle at the top of the pulse. The linear MOKE signal does not measure the entirety of the thin film, however, but measures the magnetization only in the range only slightly larger than the optical skin depth from the surface. The skin depth for Ni–Fe is typically in the range of 7–20 nm, and depends on deposition conditions. To calculate the MOKE signal from the calculated magnetization profile, the depth- and time-dependent magnetization distribution was spatially averaged, and weighted by an exponential with a decay length of the optical skin depth.

The results of this calculation are shown in Fig. 5. For a thin film (thickness less than 50 nm), the rise time of this average signal is quite fast, so both the surface (which in this model is already at H_0) and bulk move together, to the resolution of our measurement ($\sim$50 ps). Such a sample should act as a control to check the overall magnetooptical method. For thicker films, the depth-weighted average begins to rise more slowly with time, so that the 250 nm film should lag behind the 50 nm film, with a lag of $\sim$15% at 75 ps. Similarly, the bulk of a 400 nm film $\vec{M}$ should lag the surface $\vec{M}$ by 10% at 300–400 ps. Since the actual pulse has finite bandwidth ($t_{\text{rise}} \sim 150$ ps) and the dynamics are
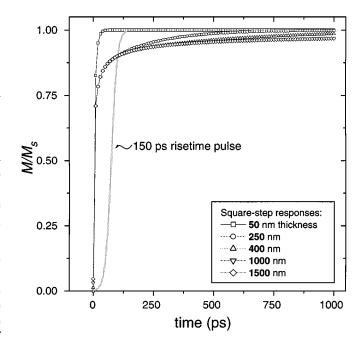

Fig. 5.   Magnetooptical response of thin films of several thicknesses, including eddy current effects, to an ideal step function external field. The 1000 and 1500 nm curves are essentially the same. A 150 ps rise-time curve (the rise time of the pulse generator used) is shown for comparison.

precessional, precluding an instantaneous response at the film surface, the difference will be slightly less.

This small difference should nonetheless be observable via our method, and is clearly *not* seen in the time traces. This suggests that eddy currents are not significantly affecting the dynamics of the magnetization vector for these film thicknesses, at least not in the manner predicted by the linear medium theory. On the other hand, the precessional dynamics of the thicker films are quite different than the thinner films, exhibiting increasing damping, likely due to eddy current effects. Work to measure thicker Ni–Fe films with similar dc magnetic properties is currently under way.

IV. CONCLUSION

The time traces show that the thicker films exhibit less precessional ringing than the 50 nm film. This increased damping may be due to increased eddy current induction. However, the incomplete rotation observed in the thicker films, and the subsequent "viscous" relaxation observed for very long ($t > 40$ ns) field pulses is *not* likely due to eddy current induction, since the time constants for the relaxation are quite long ($\sim$100 ns). These long relaxation times suggest that thermal relaxations of metastable states of the magnetization are involved in this slow rotation. However, no specific mechanism is apparent at this time, and the effect warrants further study to understand the possible ramifications for high-speed data storage applications.

The magnetization vector of both the surface (to within 1 nm) and the bulk (to within 30 nm) of the thin films studied had nearly identical temporal responses to high speed (150 ps rise time) field pulses. This would not occur if the induced eddy currents were causing gradients in the magnetization with depth, on

the scale of depth sensitivity of the linear MOKE (there could, however, be magnetization gradients on scales longer than the optical skin depth). The most likely reason for this is that the film is not truly a linear medium, but is rather a highly correlated one, due to exchange coupling. The skin effect requires that the local magnetization responds only to the local applied field. In an exchange coupled film, this is not the case, because the local magnetization is also affected by the dynamics of the surrounding magnetization, because of the exchange interaction. Consequently, the surface of the film is not free to move independently of the underlying layers and so cannot generate eddy currents to screen the applied field from the interior. Instead, the induced currents appear to affect both the surface and "bulk" equally. The linear medium model [that is, assuming $\mathbf{B}(\mathbf{r}) = \mu(r)\mathbf{H}(\mathbf{r})$] may not be appropriate for describing the high-speed response of films of moderate thickness with appreciable exchange strengths.

REFERENCES

[1] P. Arnett, R. Olsen, K. Klaassen, J. van Peppen, W. Hsiao, E. Lee, and S. Yuan, "High data rate recording at over 60 Mbytes per second," *IEEE Trans. Magn.*, vol. 35, pp. 2523–2528, Sept. 1999.

[2] T. M. Crawford, P. Kabos, and T. J. Silva, "Coherent control of precessional dynamics in thin film permalloy," *Appl. Phys. Lett.*, vol. 76, pp. 2113–2115, Apr. 2000.

[3] W. P. Jayasekara, J. A. Bain, and M. H. Kryder, "High frequency initial permeability of NiFe and FeAlN," *IEEE Trans. Magn.*, vol. 34, pp. 1438–1440, July 1998.

[4] R. Wood, M. Williams, and J. Hong, "Considerations for high data rate recording with thin-film heads," *IEEE Trans. Magn.*, vol. 26, pp. 2954–2959, Nov. 1990.

[5] J. Wu, J. R. Moore, and R. J. Hicken, "Optical pump-probe studies of the rise and damping of ferromagnetic resonance oscillations in a thin Fe film," *J. Magn. Magn. Mater.*, vol. 222, pp. 189–198, Nov. 2000.

[6] B. C. Choi, M. Belov, W. K. Hiebert, G. E. Ballentine, and M. R. Freeman, "Ultrafast magnetization reversal dynamics investigated by time domain imaging," *Phys. Rev. Lett.*, vol. 86, pp. 728–731, Jan. 2001.

[7] C. Teplin and C. Rogers, "Simultaneous MOKE and SHMOKE dynamic imaging," presented at the 8th Joint MMM-Intermag Conf., San Antonio, TX, Jan. 7–11, 2001, paper EF-07.

[8] M. R. Pufall, C. Platt, and A. Berger, "Layer-resolved magnetometry of a magnetic bilayer using the magnetooptical Kerr effect with varying angle of incidence," *J. Appl. Phys.*, vol. 85, pp. 4618–4820, Apr. 1999.

[9] P. Kabos, S. Kaka, S. Russek, and T. J. Silva, "Metastable states in large angle magnetization rotations," *IEEE Trans. Magn.*, vol. 36, pp. 3050–3052, Sept. 2000.

[10] T. J. Silva and T. M. Crawford, "Methods for determination of response times of magnetic head materials," *IEEE Trans. Magn.*, vol. 35, pp. 671–676, Mar. 1999.

[11] G. Metzger, P. Pluvinage, and R. Torguet, "Termes linéaires et quadratiques dans l'effet magnéto-optique de Kerr," *Ann. Phys.*, vol. 10, p. 5, 1965.

[12] G. Spierings, V. Koutsos, H. A. Wierenga, M. W. J. Prins, D. Abraham, and T. Rasing, "Interface magnetism studied by optical 2nd-harmonic generation," *J. Magn. Magn. Mater.*, vol. 121, pp. 109–111, Mar. 1993.

[13] T. M. Crawford, C. T. Rogers, T. J. Silva, and Y. K. Kim, "Transverse and longitudinal second-harmonic magneto-optic Kerr effect observed from $Ni_{81}Fe_{19}$ thin film structures," *IEEE Trans. Magn.*, vol. 32, pp. 4087–4089, Sept. 1996.

[14] A. Kirilyuk, T. Rasing, and M. A. M. Haast, "Probing structure and magnetism of CoNi/Pt interfaces by nonlinear magneto-optics," *Appl. Phys. Lett.*, vol. 72, pp. 2331–2333, May 1998.

[15] S. E. Russek, T. M. Crawford, and T. J. Silva, "Study of NiFe/Al/Al_2O_3 magnetic tunnel junction interfaces using second-harmonic magneto-optic Kerr effect," *J. Appl. Phys.*, vol. 85, pp. 5273–5275, Apr. 1999.

[16] R. P. Pan, H. D. Wei, and Y. K. Shen, "Optical 2nd-harmonic generation from magnetized surfaces," *Phys. Rev. B*, vol. 39, pp. 1229–1234, Jan. 1989.

[17] H. N. Bertram, *Theory of Magnetic Recording*. Cambridge, U.K.: Cambridge Univ. Press, 1994.